REPORT DOCUMENTATION PAGE

Form Approved
OMB No. 0704-0188

1. REPORT DATE *(DD-MM-YYYY)*	**2. REPORT TYPE**	**3. DATES COVERED** *(From - To)*
3/1/2012	Final Report	8/15/2010 - 8/14/2011

4. TITLE AND SUBTITLE

(DURIP 10) A TUNABLE LASER SOURCE FOR THE VALIDATION OF HOMOGENEOUS NEGATIVE REFRACTIVE INDEX MATERIALS IN THE OPTICAL REGIME

5a. CONTRACT NUMBER

5b. GRANT NUMBER
FA9550-10-1-0399

5c. PROGRAM ELEMENT NUMBER

6. AUTHOR(S)

Aklim Akyurtlu

5d. PROJECT NUMBER

5e. TASK NUMBER

5f. WORK UNIT NUMBER

7. PERFORMING ORGANIZATION NAME(S) AND ADDRESS(ES)

University of Massachusetts
600 SUFFOLK ST FL 2 S
LOWELL, MA

8. PERFORMING ORGANIZATION REPORT NUMBER

9. SPONSORING / MONITORING AGENCY NAME(S) AND ADDRESS(ES)

Air Force Office of Scientific Research
Suite 325, Room 3112
875 Randolph Street
Arlington, VA 22203-1768

10. SPONSOR/MONITOR'S ACRONYM(S)

AFOSR

11. SPONSOR/MONITOR'S REPORT NUMBER(S)
AFRL-OSR-VA-TR-2012-0944

12. DISTRIBUTION / AVAILABILITY STATEMENT

Distribution A - Approved for Public Release

13. SUPPLEMENTARY NOTES

14. ABSTRACT

This final report details the theoretical and experimental work performed on the project titled, "A Tunable Laser Source for the Validation of Homogeneous Negative Refractive Index Materials in the Optical Regime" from (AFOSR grant FA9550-10-1-0399). As part of this DURIP proposal, we have purchased a Bruker Optics Vertex 80 interferometer incorporating a broadband THz lamp and a room temperature KBr/DTGS-D301 photodetector, the AutoSeagull reflection unit and two sets of lasers (Mid-IR and CO2) to build a system for verifying the negative refractive index properties of our homogeneous, low-loss negative index materials in the mid to far-IR wavelength regime.

15. SUBJECT TERMS

16. SECURITY CLASSIFICATION OF:			**17. LIMITATION OF ABSTRACT**	**18. NUMBER OF PAGES**	**19a. NAME OF RESPONSIBLE PERSON**
a. REPORT	**b. ABSTRACT**	**c. THIS PAGE**			Harold Weinstock
U	U	U	UU	8	**19b. TELEPHONE NUMBER** *(include area code)* 703-696-8572

Standard Form 298 (Rev. 8-98)
Prescribed by ANSI Std. Z39.18

FINAL REPORT

This final report details the theoretical and experimental work performed on the project titled, "A Tunable Laser Source for the Validation of Homogeneous Negative Refractive Index Materials in the Optical Regime" from (AFOSR grant FA9550-10-1-0399). As part of this DURIP proposal, we have purchased a Bruker Optics Vertex 80 interferometer incorporating a broadband THz lamp and a room temperature KBr/DTGS-D301 photodetector, the AutoSeagull reflection unit and two sets of lasers (Mid-IR and CO_2) to build a system for verifying the negative refractive index properties of our homogeneous, low-loss negative index materials in the mid to far-IR wavelength regime.

The homogeneous negative index material based on the magnetic semiconductor based on the magnetic semiconductor $In_{2-x}Cr_xO_3$. We have shown that a strongly pronounced negative refractive index effect at ~ 27.8 μm. This effect was theoretically predicted earlier, and it is based on coexistence of the spin wave (magnon) mode with the plasmonic mode, with simultaneous negative permittivity and permeability responses. The thin films of $In_{2-x}Cr_xO_3$ are fabricated, with low stoichiometric oxygen deficiency, which is required for ferromagnetic behavior. The magnetic measurements clearly reveal the ferromagnetism with high saturation magnetization. The complex frequency-dependent refractive index is extracted from combined transmittance and reflectance data. The ordinary Hall Effect with a Van der Pauw contact geometry was used to determine the conduction carrier concentration, n_e. The structural study of the fabricated samples was done by energy dispersive spectroscopy, EDS, and the film thickness was measured by the AlphaStep profilometer instrument.

The magnetic measurements of the successful samples are performed by SQUID at 10 K and at room temperature, in hope to see expected ferromagnetic behavior. The magnetic field is applied in the sample plane. Fig. 1 shows the results of the magnetization versus applied magnetic field (M-H) curve measured at 10 K for the 0.35 μm thick of Cr:InO annealed thin films with carrier density $n_e = 0.529 \times 10^{19}$. As follows from this result, our successful samples are indeed ferromagnetic, with high saturation magnetization up to 0.6 μ_B/Cr-atoms. The measurements of the ferromagnetic thin samples with thickness 0.1 μm provided even higher saturation magnetization up to 0.8 μ_B/Cr-atoms. Since this saturation magnetization is only ~ 25% larger than magnetization 0.6 μ_B/Cr-atoms for thick samples, we can conclude that magnetization is mostly bulk effect and surface enhances ferromagnetism only to a small extent.

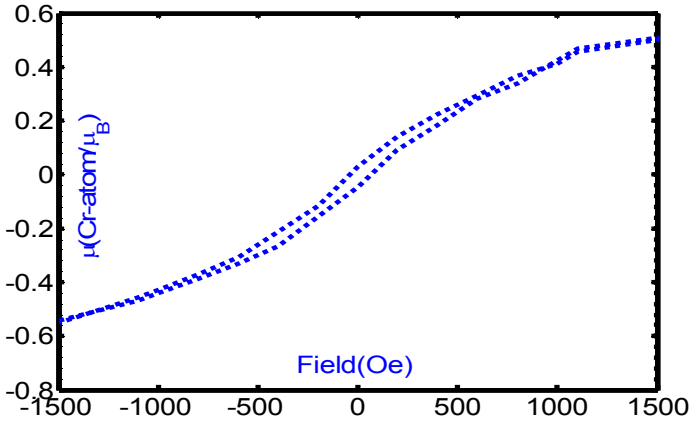

Fig. 1. Magnetization measurements indicating that the doping of Cr atoms to the In_2O_3 film and after post annealing yields a saturated magnetic moment of (0.6-0.8) μ_B per Cr atom at 10 K.

Next, the transmittance of the films were measured at normal incidence using the purchased Bruker Optics Vertex 80 interferometer incorporating a broadband THz lamp and a room temperature KBr/DTGS-D301 photodetector. This system enabled us to perform transmittance measurements of the films over the spectral range up to 40 μm. The reflectance has been measured within broad range of angle of incidence, θ, (5,10,15,20,40,50,70,80 degrees) by the AutoSeagull reflection unit.

Fig. 2(a) demonstrates, for a ferromagnetic sample, the examples of measured frequency-dependent FTIR both the reflectance coefficient R for $\theta = 5^0$, (a) $\theta = 50^0$ (b), and the transmittance coefficient. One can see, from Fig.2, the strongly pronounced *maximum* on R curves at λ_{max}~27.8 μm, and the *minimum* on the T curve at the same frequency. We assume that these extremes correspond to the limiting spin wave frequency, $\omega \sim$ 10.8 THz, on the boundary of the Brillouin zone. Indeed, this frequency is very close to the theoretical predictions [1]. Hence, the maximum at ~ 27.8 μm is a viable candidate for the desirable effect, and we extracted the refractive index within narrow range which includes this wavelength (see below).

It would be instructive to compare reflectance spectra of ferromagnetic and non-magnetic films, with the same Cr doping parameter x, but with different oxygen deficiency, δ. Fig. 3 demonstrates the typical FTIR R spectrum for the *non-magnetic* film, with the same doping x ~0.036 as the ferromagnetic film ($\delta \sim$ 0.0087) utilized in Fig. 2, but with the oxygen deficiency, $\delta \sim$ 0.06, outside of the required range ($1.6\times10^{-4} \le \delta \le 10^{-2}$) which is required for the ferromagnetic indirect spin-spin coupling [2]. One can see, in contrast to ferromagnetic film, that the non-magnetic film possesses *no maximum* in region 27-28 μm. Such behavior is expected, since the spin waves (magnons) which are responsible for the maximum are not presented in this specific film0. Moreover, the non-magnetic R spectrum, at 27.8 μm, shows a *minimum* instead of a *maximum*, and R is much *smaller* than R for the ferromagnetic film. One can conclude that the strongly pronounced peaks on R curve, with simultaneous extremely high reflectance R > 0.8, are the signatures of the magnon-plasmon resonance in magnetic semiconductors.

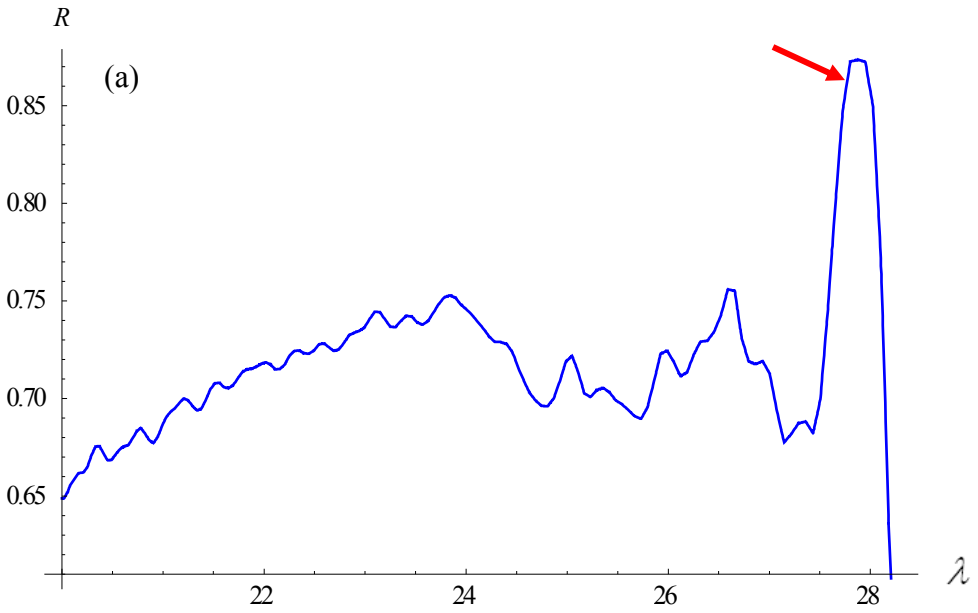
R
(a)
0.85
0.80
0.75
0.70
0.65
22
24
26
28
λ

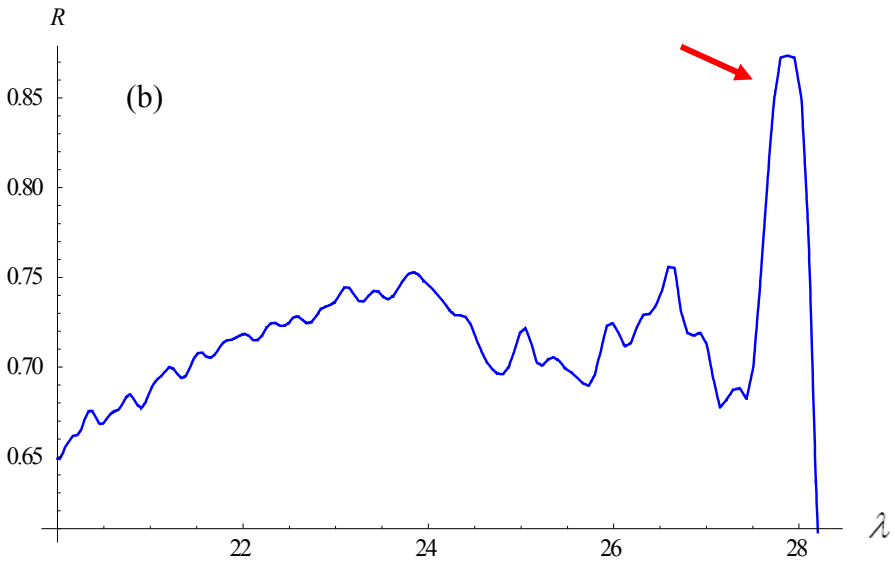
R
(b)
0.85
0.80
0.75
0.70
0.65
22
24
26
28
λ

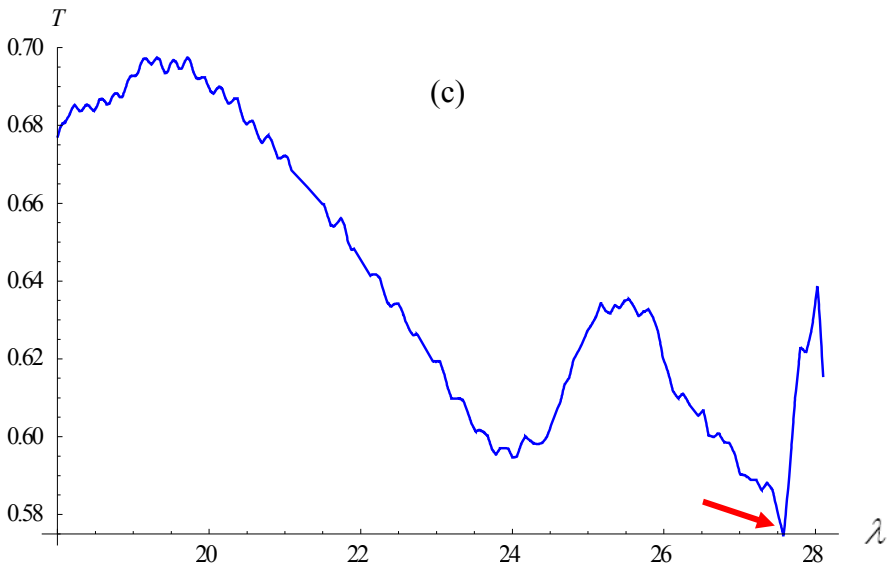

Fig. 2. Reflectance coefficient, R, and transmittance coefficient, T, of the *ferromagnetic* thin film of In_{2-x} Cr_x $O_{3-\delta}$, x~0.036, $\delta \cong 0.0087$, for different angles of incidence: a) R, θ=5°, b) R, θ=50°, c) T, θ=0°,. Red arrow points to magnon-plasmon overlapping resonance at ~ 27.8 μm, which corresponds to a maxima of R and a minima of T.

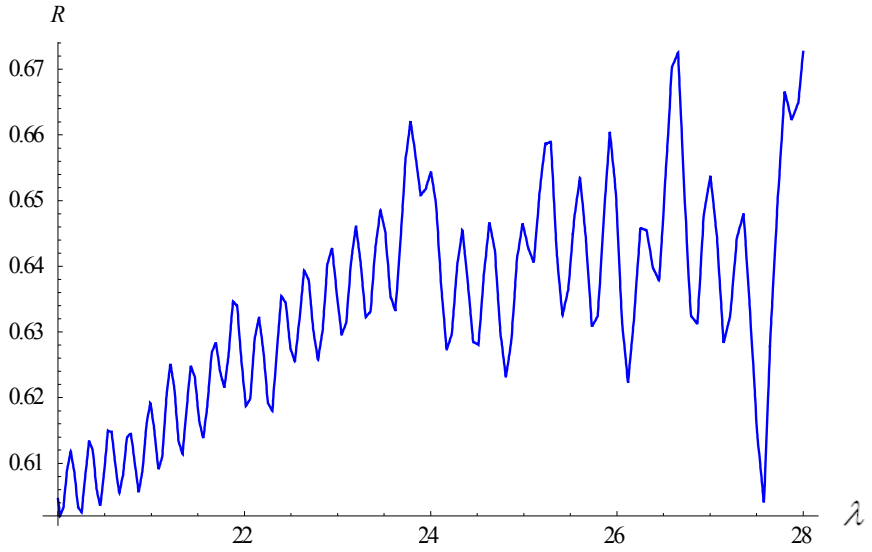

Fig. 3. Reflectance coefficient, R, of the *nonmagnetic* thin films of In_{2-x} Cr_x $O_{3-\delta}$, x~0.036, δ ~ 0.06, for angle of incidence θ=50°.

Extraction Methodology

Even though FTIR measurements do not provide the *phase* of reflected and transmitted waves, the optical constants, or real and imaginary parts, $n_1(\lambda)$ and $n_2(\lambda)$, of a complex refractive index, $n(\lambda) = n_1(\lambda) + in_2(\lambda)$, can still be reliably extracted from the combined reflection and transmission amplitudes, $R(\lambda,\theta)$ and $T(\lambda,\theta)$, measured at sequence of incident angles $\theta_1, \theta_2, ...\theta_l$, if this sequence covers a wide range of angles [3]. The method of the extraction of $n(\lambda)$ which was used for this project, is based on the following formulations. Obviously, each theoretically calculated curve with fixed θ for reflection and transmission $R_{TH}(\theta, n_1(\lambda), n_2(\lambda))$, $T_{TH}(\theta, n_1(\lambda), n_2(\lambda))$, should depend on $n_1(\lambda)$ and $n_2(\lambda)$. Hence, within a narrow region, close to the specific wavelength of an interest, $\lambda \sim \lambda_{ext}$, it is possible to fit calculated amplitudes $R_{TH}(\theta, n_1(\lambda), n_2(\lambda))$, $T_{TH}(\theta, n_1(\lambda), n_2(\lambda))$ to experimental data, $R(\lambda,\theta)$ and $T(\lambda,\theta)$, in order to extract the couples of optical constants $\{n_1(\theta_i, \lambda), n_2(\theta_i, \lambda)\}$ which depend on the incident angle $\theta = \theta_i$. Afterwards, one can analyze which couple $\{n_1, n_2\}$ is the same for *all* R-T amplitudes, or for the whole set $\theta = \theta_i$, and this solution should correspond to true refractive index, $n_1(\lambda_{ext})$, $n_2(\lambda_{ext})$.

In the calculation of the reflection–transmission amplitudes, $R_{TH}(\theta, n_1(\lambda), n_2(\lambda))$ and $T_{TH}(\theta, n_1(\lambda), n_2(\lambda))$, we have followed the classical Born's method [3] of characteristic reflection-transmission matrix of a stratified medium. This medium is the film which covers the silicon carbide substrate with thickness ~ 250 μm and permittivity $\varepsilon_s \sim 3.38 + i0.0034$ (both extrapolated from data of Ref. 4 and directly measured at wavelength ~28 μm).

The appropriate extracted refractive index band in vicinity of the magnon-plasmon resonance, at $\lambda_{max} \sim 27.8$ μm, is shown in Fig. 4. One can see, from Fig. 4, that refractive index becomes negative within narrow band with Re(n) ~ -2.0, $\mathrm{Im}(n) \approx 2.0$, which corresponds to figure of merit, $FOM \sim 1$. Hence, due to negative refractive index effect at ~ 27.8 μm, we can conclude that this wavelength consistently corresponds to assumed plasmon-magnon resonance.

As follows from Fig.4, the positive refractive index, Re(n) ~ 1.0 and Im(n) ~ 10.0, outside of the negative refractive index band. The magnitude of this refractive index can be explained from the Drude plasmon permittivity ε [5],

$$\varepsilon(\omega) = \varepsilon_\infty \left(1 - \frac{\omega_D^2}{(\omega^2 + i\gamma\omega)}\right) \qquad (1),$$

where the Drude frequency, $\omega_D \sim 310.5$ THz, corresponds to concentration of electrons ($N \sim 2.7 \times 10^{20}$ (1/cm^3)) in the conduction band for experimental oxygen deficiency $\delta \sim 0.0087$; $\varepsilon_\infty \sim 0.8$, and γ is the losses in plasmonic subsystem. Due to the lack of magnetic response ($\mu \sim 1$) outside the narrow band, at the boundary of the Brillouin zone [1, 6],

(which coincides approximately with the negative refractive band), the refractive index, outside the band, can be approximated as $n = \sqrt{\varepsilon}$. Since the Drude frequency is much larger than the frequency where the negative refractive index band is located ($\omega_D >> \omega_{TH}$), the calculated real part of the Drude permittivity is negative: Re(ε) ~ -100.0. The appropriate real and imaginary parts of the index of refraction are as follows: Re(n) ~ 1.0 and Im(n) ~ 10.0. Hence, as one can see from Fig. 4, real and imaginary parts of refractive index, as predicted by Drude theory, are on the same order of magnitude with experimental refractive index in the vicinity of the negative refractive index band. The behavior of $n(\lambda)$ is fully consistent both within and outside the negative refractive index band with the theoretical predictions [1, 7].

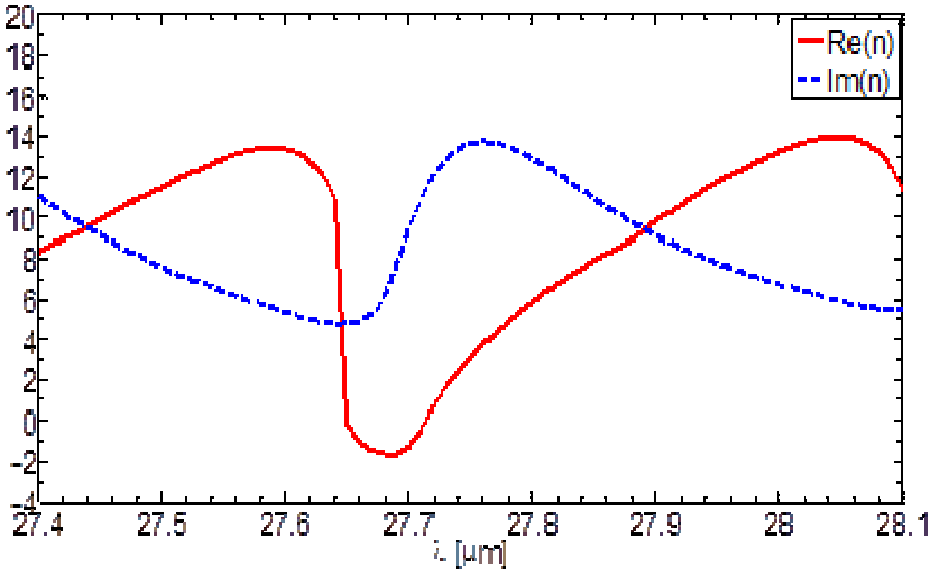

Fig. 4 Extracted refractive index n=Re(n)+iIm(n) in the vicinity of the plasmon-magnon resonance of the *ferromagnetic* film $In_{2-x}Cr_xO_{3-\delta}$, x~0.036, δ ~ 0.0087.

In conclusion, the negative refractive index band parameters of ferromagnetic Cr-doped indium oxide thin films (i.e. wavelength and bandwidth) are fully consistent with predicted ones in Ref. 27, and the measured electric and magnetic properties of Cr-doped IO are close to those reported in literature [29]. Specifically, the experimentally verified negative refractive index narrow band, with width, $\Delta\lambda/\lambda_{max}$~0.005, is located at the limiting frequency of the magnon spectra, λ_{max}~27.8 μm, with Re(n)~ -2.0, Im(n) ~2.0. The theoretical prediction of Ref. 10 provides the negative refractive index band at λ_{max} ~ 30.0 μm with the estimated width, $\Delta\lambda/\lambda_{max}$~0.001-0.1, and the refractive index, Re(n)~ -2.5, Im(n) ~1.0. These predictions are in close proximity to the extracted experimental parameters reported above.

Conclusions

As a result of this project, we have been able to validated the negative index properties of the homogeneous negative index material based on the magnetic semiconductor (specifically, Cr doped IO) are considered where the effect is due to the coexistence of the spin wave mode with the plasmonic mode. Both of these modes are activated by the e.m. field of the light with simultaneous permittivity and permeability responses within some frequency band, which ensures the negative refractive index within the frequency band close to the boundary of the Brillouin zone of the magnon spectra. Based on these studies presented herein, we believe that natural homogeneous magnetic semiconductors with well-pronounced negative refractive index band can be promising in future applications. The advantages of these natural materials compared with inhomogeneous composite metamaterials are their optical isotropy, and the fact that the optical constants, ε, μ, n are true physical variables defined on the atomic level, rather than some "effective" parameters. Next, we will also use the Mid-IR and CO_2 lasers to validate the negative index properties on similar homogeneous Negative Index material systems based on Fe and Ni, as well as on using parametric loss suppression on these materials (which has been funded by AFOSR).

REFERENCES

[1] A.G. Kussow and Alkim Akyurtlu, Phys. Rev. B, **78**, 205202 (2008).
[2] J. Philip, A. Punnoose, B.J. Kim, K.M. Reddy, S. Layne, J.O. Holmes, B. Satrati, P.R. Leclair, T.S. Santos and J.S. Moodera, Nature Materials **5,** 298 (2006).
[3] M.Born and E.Wolf, Principles of Optics (Pergamon, Oxford, 1999).
[4] W.G. Spitzer, D. Kleinman and D.Walsh, Phys. Rev. 113, 128 (1959).
[5] P. O. Nilsson, Applied Optics, 7, 441 (1968).
[6] A.G. Kussow and A. Akyurtlu, J. Nanophoton., 4, 043514 (2010).
[7] S .Zh. Karazhanov, P. Ravindran, P. Vajeeston, A. Ulyashin, T. G. Finstad, and H. Fejellvag, Phys. Rev. B 76 , 075129 (2007).
[8] David J. Payne, A. Emmanuelle Marquis, Chem. Mater. **23,** 1085 (2011).